PHARMACIA

Pharmacia 71: 1–18
DOI 10.3897/pharmacia.71.e132095

Research Article

Molecular simulation-based evaluation of anti-inflammatory properties of natural compounds derived from tobacco (*Nicotiana tabacum* L.): Computational multi-target approaches

Vinda Maharani Patricia[1], Aulia Fikri Hidayat[1], Taufik Muhammad Fakih[1]

1 *Department of Pharmacy, Faculty of Mathematics and Natural Sciences, Universitas Islam Bandung, Jl. Ranggagading, Bandung, 40116, Indonesia*

Corresponding author: Vinda Maharani Patricia (vinda.maharani@unisba.ac.id)

Received 15 July 2024 ♦ **Accepted** 25 September 2024 ♦ **Published** 7 November 2024

Citation: Patricia VM, Hidayat AF, Fakih TM (2024) Molecular simulation-based evaluation of anti-inflammatory properties of natural compounds derived from tobacco (*Nicotiana tabacum* L.): Computational multi-target approaches. Pharmacia 71: 1–18. https://doi.org/10.3897/pharmacia.71.e132095

Abstract

Various components of the tobacco plant (*Nicotiana tabacum* L.) have undergone pharmacological assessment to highlight their traditional role in addressing different health conditions. The anti-inflammatory properties of thirteen natural substances were investigated through the use of molecular docking conducted with AutoDock 4.2.6 Tools and Molecular Dynamics Simulations (MDS) executed with GROMACS 2016.3. ADME characteristics were assessed using SwissADME (absorption, distribution, metabolism, and excretion). Chlorogenic acid and rutin, plant-derived natural compounds, showed substantial binding tendencies with cyclooxygenase-1 (COX-1), phosphodiesterase-4 (PDE4), cyclooxygenase-2 (COX-2), phosphodiesterase-7 (PDE7), interleukin-17A (IL-17A), interleukin-1 beta (IL-1β), tumor necrosis factor-alpha (TNF-α), prostaglandin E2 (PGE2), and prostaglandin F synthase. Rutin emerged as the most notable among the tested compounds (docking energy: −11.0 kcal/mol against PDE7 and prostaglandin F synthase). Chlorogenic acid also displayed substantial and noteworthy binding energies of −9.4 kcal/mol with PDE4 and PDE7 receptors. Consequently, these investigated natural compounds could potentially serve as agents that reduce inflammation and require additional in vitro and in vivo studies to aid the creation of new anti-inflammatory drugs.

Keywords

tobacco (*Nicotiana tabacum* L.), natural products, anti-inflammatory properties, computational multi-target, drug candidates

Introduction

Historically, traditional tobacco, now recognized as *Nicotiana rustica*, was utilized for medicinal purposes (Popova et al. 2020). Initially masticated, similar to coca leaves, this practice gradually integrated into the habits of European settlers and disseminated globally. Another native approach to tobacco consumption – sniffing powdered leaves – likewise gained traction over time (Drapal et al. 2022). Despite nicotine's role in fueling tobacco's popularity, a sophisticated biosynthetic mechanism within tobacco plants produces a plethora of distinct compounds.

PENSOFT.

Presently, ordinary tobacco (*Nicotiana tabacum* L.) is predominantly linked with the manufacturing of products for consumers. Nonetheless, like many botanical counterparts, tobacco demonstrates efficiency in generating various beneficial secondary metabolites (Ahrazem et al. 2022). Consequently, the tobacco species, coupled with its agricultural expertise, emerges as a leading force in the biological economic system revolution, functioning as a non-edible resource and a carbon-negative entity, well-suited for large-scale industrial applications. (Secchi et al. 2016).

Nicotiana tabacum L. is defined as an allotetraploid organism with a genome size of 4.5 gigabases (Gb), rendering it one of the most expansive and gene-rich among routinely grown agricultural plants, about fivefold greater than the genomes of potatoes and tomatoes (Zhang et al. 2022b). With a gene count of 90,000, tobacco potentially harbors remarkable capabilities for generating biologically intricate compounds available in substantial quantities (Camlica and Yaldiz 2021). Estimations suggest that tobacco tissues comprise roughly 5700 distinct chemical elements, including alkaloids, carboxylic acids, carbohydrates, inorganic compounds, isoprenoids, nitrogen-based substances, phenolics, pigments, and sterols. Consequently, based on numerous studies, tobacco plants could serve as a significant component in addressing inflammatory conditions (Bensalah et al. 2009; Zhang et al. 2022a; Leal et al. 2023).

Inflammation represents the vascular tissues' biological reaction to detrimental triggers, involving pain, increased vascular permeability, membrane structure changes, and protein denaturation. Various factors, including microbial, physical, and chemical agents, can trigger inflammation as a response to damaged body cells (Fioranelli et al. 2021). Globally, nonsteroidal anti-inflammatory drugs (NSAIDs) are extensively utilized. However, their use is associated with significant adverse impacts on the digestive system, liver, and kidneys, posing challenges in their administration across different therapies (Moore et al. 2023). As a result of the significant adverse effects linked to NSAID treatment, there is an increasing interest in natural herbal remedies. Consequently, numerous researchers are increasingly focusing on exploring and developing herbal medicines as improved treatments for anti-inflammatory conditions (Yasmin et al. 2015).

Furthermore, the current imperative lies in the quest for natural anti-inflammatory compounds that regulate the inflammatory response without significant negative effects. Investigators have noted the anti-inflammatory attributes of *Nicotiana tabacum* L., evidenced by its extract's ability to mitigate conditions associated with oxidative effect and inflammation induced by *Rhodococcus fascians* infection, albeit with a potency lesser than that of pure standards (Nacoulma et al. 2012). Moreover, separate studies have highlighted the considerable anti-inflammatory effectiveness of tobacco seed oils that has been documented; these oils inhibit the production of pro-inflammatory cytokines such as IL-1β, IL-6, and TNF-α by interfering with the mitogen-activated protein kinase (MAPK) signaling pathway (Gu et al. 2022). Additional research has unveiled a novel role for tobacco cembranoids as analgesic agents in rats, attenuating peripheral inflammation and thereby reinforcing therapeutic modulation of the cholinergic system as a strategy for pain control (Rivera-García et al. 2024).

Improving chronic inflammation management and enhancing patient quality of life depend on the development of innovative treatments for inflammation. Researchers are tapping into natural resources, such as plants, to create new drugs with fewer side effects (Chakraborty et al. 2021). This study sought to discover potential natural anti-inflammatory compounds that engage with different inflammatory receptors or mediators to enhance therapeutic outcomes. This is crucial for facilitating their use in therapy at lower doses (Radovanović et al. 2023). To achieve this goal, computational analyses were conducted, including screening, molecular docking, and dynamics simulations of phytochemicals extracted from *Nicotiana tabacum* L. This marks the first exploration of the therapeutic potential of bioactive compounds derived from tobacco plants. Thus, based on the findings of this study, the discovery of novel candidate compounds in *Nicotiana tabacum* L. suggests their potential as potent anti-inflammatory drugs that can enhance anti-inflammatory effects by targeting different receptors.

Materials and methods

Bioactive compound preparation

The research involved selecting thirteen natural compounds sourced from tobacco (*Nicotiana tabacum* L.) through various solvents (CH_2Cl_2 (dichloromethane)/MeOH (methanol) (4:1, v/v), CH_2Cl_2 (dichloromethane), EtOH (ethanol), MeOH (methanol), C_6H_{14} (hexane), MeOH (methanol)/H_2O (water) (70:30, v/v), and H_2O (water)) and extraction techniques (microfractionation) from prior studies (Table 1) (Laszlo et al. 2022). The 2D structures and key compounds derived from tobacco were sourced using their SMILES (Simplified Molecular Input Line Entry System) IDs from the PubChem database, accessible at https://pubchem.ncbi.nlm.nih.gov/ (Laszlo et al. 2022). The SMILES IDs were transformed into 3D PDB (Protein Data Bank) files through the NovoPro Bioscience server, available at https://www.novoprolabs.com/tools/smiles2pdb to facilitate subsequent docking and molecular simulation investigations (Amaro et al. 2018). The ligand file underwent energy minimization via BIOVIA Discovery Studio 2022 Client 22.1 to ensure it achieved a stable, low-energy conformation, reducing strain and optimizing geometry for accurate molecular interactions in further simulations (BIOVIA 2017). The macromolecular system was modeled using the CHARMm (Chemistry at HARvard Macromolecular Mechanics) force field, applying empirical energy functions for accurate simulations (Vanommeslaeghe et al. 2010).

Table 1. List of bioactive compounds sourced from *Nicotiana tabacum* L. and their chemical details retrieved from the PubChem database.

Bioactive Compound	PubChem Identifier	Chemical Formula	Molecular Weight	2D Structure	Canonical SMILES
Anabasine	205586	$C_{10}H_{14}N_2$	162.23 g/mol	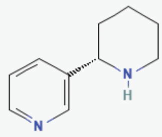	C1CCNC(C1)C2=CN=CC=C2
Anatabine	11388	$C_{10}H_{12}N_2$	160.22 g/mol	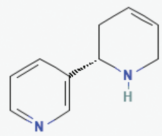	C1C=CCNC1C2=CN=CC=C2
Chlorogenic Acid	1794427	$C_{16}H_{18}O_9$	354.31 g/mol	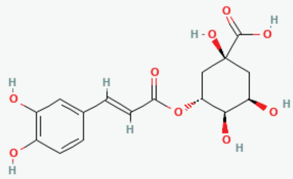	C1C(C(C(CC1(C(=O)O)O)OC(=O)C=CC2=CC(=C(C=C2)O)O)O)O
Cotinine	854019	$C_{10}H_{12}N_2O$	176.21 g/mol	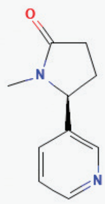	CN1C(CCC1=O)C2=CN=CC=C2
Ferulic Acid	445858	$C_{10}H_{10}O_4$	194.18 g/mol	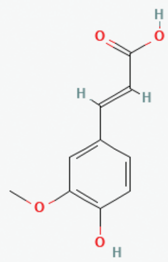	COC1=C(C=CC(=C1)C=CC(=O)O)O
Linoleic Acid	5280450	$C_{18}H_{32}O_2$	280.4 g/mol	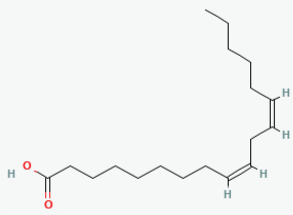	CCCCCC=CCC=CCCCCCCCC(=O)O
Myosmine	442649	$C_9H_{10}N_2$	146.19 g/mol	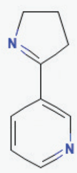	C1CC(=NC1)C2=CN=CC=C2
Niacinamide	936	$C_6H_6N_2O$	122.12 g/mol	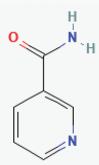	C1=CC(=CN=C1)C(=O)N

Bioactive Compound	PubChem Identifier	Chemical Formula	Molecular Weight	2D Structure	Canonical SMILES
Nicotine	89594	$C_{10}H_{14}N_2$	162.23 g/mol	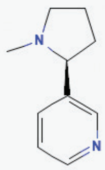	CN1CCCC1C2=CN=CC=C2
Nicotinic Acid	938	$C_6H_5NO_2$	123.11 g/mol	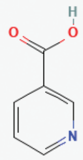	C1=CC(=CN=C1)C(=O)O
Norcotinine	413	$C_9H_{10}N_2O$	162.19 g/mol	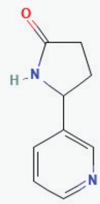	C1CC(=O)NC1C2=CN=CC=C2
Nornicotine	412	$C_9H_{12}N_2$	148.20 g/mol	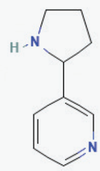	C1CC(NC1)C2=CN=CC=C2
Rutin	5280805	$C_{27}H_{30}O_{16}$	610.5 g/mol	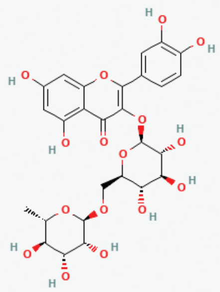	CC1C(C(C(C(O1)OCC2C(C(C(C(O2)OC3=C(OC4=CC(=CC(=C4C3=O)O)O)C5=CC(=C(C=C5)O)O)O)O)O)O)O)O

Macromolecule target preparation

The COX-2 macromolecule is a type of protein that aids in the generation of prostaglandins associated with inflammation and pain. Its human crystal structure (PDB ID: 5F1A) is sourced from the PDB repository at https://www.rcsb.org/structure/5F1A (Lucido et al. 2016). Following this, water (HOH) molecules and heteroatoms (HETATM) were excluded from the initial PDB files, and energy minimization was conducted using the CHARMm force field through BIOVIA Discovery Studio 2022 Client 22.1 (BIOVIA 2017). This process aimed to pinpoint the specific region on the receptor where ligands have the potential to attach and interact with the amino acid residues. The active site analysis of 5F1A was performed using BIOVIA Discovery Studio 2022 Client 22.1, allowing the recognition of essential amino acids vital for the binding site docking of the chosen natural compounds.

Receptor-ligand interaction using AutoDock 4.2.6 Tools

In AutoDock 4.2.6 Tools, undesirable elements such as cofactors, water molecules, and other compounds were eliminated from the macromolecule structure (Forli et al. 2012). Subsequently, hydrogen atoms were added, charges and atom types were assigned, and the geometry was optimized. To facilitate ligand binding, multiple conformations and tautomers were generated to suit the receptor's binding site. A grid box was then defined, covering the docking area of interest. This box sets the dimensions and resolution for the grid points, essential for calculating the energy interactions between the ligand and the receptor. The grid points' coordinates (x, y, z) were configured as 64 × 60 × 60, with a separation of 0.375 Å. The central grid coordinates for various receptors were as follows: COX-1 (−20.975, 50.155, 10.484) (Sidhu et al. 2010), COX-2 (41.968, 23.972, 240.058) (Lucido et al. 2016), PDE4 (96.093, 62.876, 19.445) (Wang et al. 2007), PDE7 (−0.674, 51.594, 22.365) (Wang et al. 2005), IL-17A (79.829, −44.902, −-46.037) (Liu et al. 2016), TNF-α (−19.163, 74.452, 33.837) (He et al. 2005), IL-1β (8.066, 25.055, −9.87), prostaglandin E2 (−15.069, −6.345, −5.058) (Schiele et al. 2015), and prostaglandin F synthase (−3.359, −21.719, 12.506) (Komoto et al. 2004).

Afterward, the scoring function, docking algorithm, and output settings were kept at their default values. The Lamarckian Genetic Algorithm (LGA) was employed, along with an empirical free energy equation, to determine the ligand's orientation and positioning within the macromolecule's binding site (Mohapatra et al. 2015). The scoring function assessed the ligand's suitability for the macromolecule and predicted its binding affinity (ΔG) using a formula incorporating terms such as ΔG_{gauss}, $\Delta G_{repulsion}$, ΔG_{hbond}, $\Delta G_{hydrophobic}$, and ΔG_{tors}, each representing different aspects of molecular interaction. Upon successful execution, AutoDock 4.2.6 Tools generated ligand and receptor files, set up the docking grid, and documented the parameters applied (Forli et al. 2012). Settings like crossover rate, energy evaluations, mutation rate, population size, and step size were configured based on the size and complexity of the molecules involved. Additionally, the number of LGA runs was capped at 100. Subsequently, the docking poses were examined, ranked by their scores, and visualized using BIOVIA Discovery Studio 2022 Client 22.1 (BIOVIA 2017). This final step included comparison with control data (binding affinity data and reference ligands) to validate the results.

ADMET and drug-likeness prediction

The SwissADME web-based platform (http://www.swissadme.ch/), offered by the Swiss Institute of Bioinformatics (SIB) in Lausanne, Switzerland, was utilized to computationally predict the bioavailability, drug suitability, and pharmacokinetic profiles of the selected natural compounds (Daina et al. 2017). In addition, further toxicity was evaluated using the pkCSM online tool (https://biosig.lab.uq.edu.au/pkcsm/) (Pires et al. 2015).

Receptor-ligand dynamics using Gromacs 2016.3

A 500 ns Molecular Dynamics Simulation (MDS) was performed on the COX-2-Chlorogenic acid, COX-2-Rutin, and COX-2-Celecoxib complexes utilizing GROMACS version 2016.3 software (Aragones et al. 2013, Abraham et al. 2015). Celecoxib was utilized in this study as a comparison drug, which is already commercially available and known to be an effective COX-2 inhibitor, allowing a comparison between its effects and those of the test compounds, chlorogenic acid, and rutin (Jin et al. 2020). Additionally, COX-2 was simulated in water as a comparison. The pdb2gmx package (a tool in the GROMACS software) was utilized to generate structural topology data for COX-2, applying the CHARMM27 all-atom force field to assign molecular parameters such as bond types, angles, and dihedrals (Sapay and Tieleman 2011). Topology files for chlorogenic acid, rutin, and celecoxib ligands were acquired from the SwissParam server (http://www.swissparam.ch/) (Bugnon et al. 2023). To solvate the system, a triclinic box filled with water was generated, and Na+ and Cl− ions were added for stabilization. A total of 98 Na+ ions and 102 Cl− ions were utilized for neutralization at a concentration of 0.15 molar. The solvated box contained dimensions of 10.22436 nm × 10.22436 nm × 10.22436 nm for the COX-2-chlorogenic acid, COX-2-rutin, and COX-2-celecoxib complexes, respectively. Following energy minimization, the system underwent equilibration using two-step ensembles (Number of particles (N), Volume (V), and Temperature (T) = NVT and Number of particles (N), Pressure (P), and Temperature (T) = NPT). The steepest descent algorithm employed 5000 steps to control and stabilize the system's temperature and pressure throughout the simulation. Equilibrium parameters included a temperature of 300 K, a pressure of 1.0 bar, and an equilibration time of 100 ps. Analysis utilized GROMACS tools: gmx rms for RMSD (root-mean-square deviation) calculation, gmx rmsf for RMSF (root-mean-square-fluctuation) calculation, gmx gyrate for Rg (radius-of-gyration) calculation, and gmx hbond to assess hydrogen bond formation during interaction. XMGRACE version 5.1 generated 2D plots (Turner 2005).

Molecular mechanics with poisson–boltzmann surface area (MM-PBSA) method

Kumari and co-researchers (2014) applied an estimation technique in their study to predict the binding free energies of particular complexes (Kumari et al. 2014). This technique is based on the molecular mechanics-poisson-boltzmann surface area (MM-PBSA) method and utilizes specialized software developed for assessing solvation characteristics in biomolecules such as proteins and complex systems (Genheden and Ryde 2015). The approximation incorporates two primary elements in the free energy calculation, omitting the entropic factor. The first element addresses the potential energy in a vacuum (ΔG_{MM}), which includes both bonded terms (such as angle, bond, and torsion energies) and non-bonded terms like van der Waals (ΔG_{VDW}) and electrostatic interactions ($\Delta G_{Coulomb}$). The second element ($\Delta G_{Solvation}$) considers the influence of solvation, combining both polar (ΔG_{Polar}) and non-polar ($\Delta G_{Nonpolar}$) solvation energies. This calculation utilizes an implicit solution model. In the MM-PBSA approach, the free energy equation is expressed as follows:

$$\Delta G = \text{potential energy in a vacuum } (\Delta G_{MM}) + \text{second element } (\Delta G_{Solvation})$$

where

$$\Delta G_{MM} = \text{electrostatic interactions } (\Delta G_{Electrostatic\ pot}) + \text{van der Waals } (\Delta G_{VDW})$$

The solvation energy indicates the energy needed to move a solute from a vacuum into a solvent and is defined as the total of polar and nonpolar energies.

$\Delta G_{Solvation}$ = polar solvation energy (ΔG_{Polar}) + non-polar solvation energy ($\Delta G_{Nonpolar}$)

The polar component is primarily linked to the creation of permanent dipoles, while the nonpolar surface involves permanent dipoles and relates to the solute's charge distribution. In the MM-PBSA calculation, ionic strength was regulated by introducing 0.150 M of NaCl. The configuration settings defined 10 grid points per A^2, with a maximum of 50,000 iterations for the linear Poisson–Boltzmann solver.

Results and discussion

Receptor-ligand interaction using AutoDock 4.2.6 Tools

To assess the binding affinity, molecular docking techniques were employed to predict how compounds bind to each receptor. The analysis covered multiple interactions such as hydrogen bonds, hydrophobic forces, electrostatic interactions, and other connections established between the compounds and the target residues (Ahmad et al. 2018). The results are presented in Tables 2, 3.

Inhibitors of COX-1 and COX-2 are commonly focused on in the creation of anti-inflammatory and analgesic medications. The rutin compound exhibits moderate binding affinity towards COX-1, exhibiting a binding energy of −8.6 kcal/mol (Park et al. 2022). The interaction involves hydrogen bonds with residues ARG120:NE, ARG120:NH2, TYR355:OH, SER353:O, ALA527:CA, and SER530:CB of COX-1, along with twelve hydrophobic interactions with amino acid residues SER353:CA, ILE523:CD1, ILE89, LEU115, VAL116, VAL349, LEU352, ILE523, ALA527, VAL349, LEU352, and ALA527. The docking outcomes with COX-1 are detailed in Table 2. Conversely, a moderate to strong binding affinity is noted with COX-2, displaying a binding energy of −9.2 kcal/mol. Seven hydrogen bondings are formed against residues ARG120:NE, TYR355:OH, TYR385:OH, TYR355:OH, VAL349:O, TYR355:OH, and TYR385 from COX-2, along with ten hydrophobic contacts with residues VAL523:CG1, VAL523:CG2, VAL523:CG2, TYR385, ARG120, LEU352, LEU352, LEU352, MET522, and VAL523. These interactions potentially stabilize the complex, as outlined in Table 3.

The study's findings suggest that the examined compound demonstrates stronger inhibition towards COX-2 than COX-1. This indicates a greater binding affinity or selectivity for COX-2, implying that the compound could be more effective in targeting COX-2-related inflammatory processes while exhibiting weaker interactions with COX-1. This is advantageous to minimize adverse effects linked to COX-1 inhibition, including gastric irritation and ulcers. Rutin, the compound in question, also shows significant binding affinity with COX-2 and prostaglandin E2 (PGE2) proteins, which are key natural mediators of inflammation linked to COX-2. These findings hint at the potential of the investigated compound to enhance its anti-inflammatory effects through interactions with PGE2 and binding to COX-2, leading to decreased production. In a similar context of inflammatory regulation, the roles of PDE4 and PDE7 enzymes, which are involved in the breakdown of cyclic adenosine monophosphate (cAMP) – a secondary messenger essential for many cellular responses – have been investigated. Inhibitors aimed at these enzymes, PDE4 and PDE7, are under examination as potential therapies for several inflammatory disorders, including asthma, chronic obstructive pulmonary disease (COPD), psoriasis, and rheumatoid arthritis, suggesting a broad therapeutic application in inflammation management (Huang et al. 2023).

The compounds chologenic acid and rutin in this investigation displayed notable affinities for PDE4, registering binding energies of approximately −9.4 kcal/mol and −9.8 kcal/mol, respectively. Rutin formed hydrogen bonding against residues such as ASN533:OD1, THR545:OG1, ASP530:OD2, MET569:SD, and SER580:O of PDE4, while interacting with five hydrophobic residues, including ILE548:CG2, ILE548:CD1, PHE584, HIS372, and MET485. On the other hand, chlorogenic acid established hydrogen bonds with ASP530:OD2, HIS416:NE2, GLU442:OE2, SER420:CA, and TYR371:OH residues of PDE4, alongside interacting with four hydrophobic residues, namely TYR371, PHE584, LEU531, and ILE548. Conversely, rutin exhibited a notable binding affinity towards PDE7, registering a binding energy of −11.0 kcal/mol. This interaction included the establishment of nine hydrogen bonds against PDE7 residues such as ASN260:ND2, ILE323:N, GLN413:NE2, HIS212:NE2, ASP362:OD2, GLN413:OE1, THR321:O, ASP253:OD1, and ASP253:OD1 at the active binding site. Building on these findings, numerous research works have highlighted the potential of bioactive constituents derived from the tobacco plant (*Nicotiana tabacum* L.) extracts in impeding PDE activity. These results present a promising avenue for addressing various inflammatory conditions, as detailed in Table 2.

IL-17A, an important component of the IL-17 cytokine family, is crucial for the regulation of inflammation, immune responses, and cellular signaling pathways. As the primary cytokine produced by Th17 cells, IL-17A enhances the host's defenses against infections and contributes to autoimmune disorders (von Stebut et al. 2020). Research on IL-17A interactions with phytochemicals indicates notable binding affinities, with chlorogenic acid exhibiting −8.0 kcal/mol and rutin showing −9.7 kcal/mol. Chlorogenic acid forms eight hydrogen bonds with IL-17A residues, including ASN36:N, TRP67:N, LEU97:O, LEU97:O, VAL65:O, VAL65:O, PRO63:CD, and VAL65:O, while also establishing one hydrophobic contact with residue ILE96:CD1. Conversely, rutin interacts through seven hydrogen bonds with IL-17A residues LEU97:N, GLU95:O, LEU97:O, GLU95:OE2, LEU97:O, PRO63:CD, and GLU95:O, in addition to four hydrophobic contacts involving residues ILE96:CA, LEU97, LEU97, and ILE96.

Table 2. The docking analysis results involving bioactive compounds and specific receptors, including COX-1, PDE4, COX-2, PDE7, IL-17A, IL-1β, TNF-α, prostaglandin E2, and prostaglandin F synthase.

Macromolecule Target	Bioactive Compound	Binding Energy (kcal/mol)
3N8Z (COX-1)	Anabasine	−6,7
	Anatabine	−6,8
	Chlorogenic Acid	**−7,7**
	Cotinine	−5,1
	Ferulic Acid	−7,0
	Linoleic Acid	−5,8
	Myosmine	−5,9
	Niacinamide	−5,8
	Nicotine	−6,7
	Nicotinic Acid	−5,6
	Norcotinine	−7,0
	Nornicotine	−6,4
	Rutin	**−8,6**
5F1A (COX-2)	Anabasine	−6,9
	Anatabine	−7,0
	Chlorogenic Acid	**−8,4**
	Cotinine	−5,6
	Ferulic Acid	−7,2
	Linoleic Acid	−5,9
	Myosmine	−6,4
	Niacinamide	−5,8
	Nicotine	−6,3
	Nicotinic Acid	−5,6
	Norcotinine	−6,4
	Nornicotine	−6,5
	Rutin	**−9,2**
2QYK (PDE4)	Anabasine	−6,4
	Anatabine	−6,5
	Chlorogenic Acid	**−9,4**
	Cotinine	−7,0
	Ferulic Acid	−7,4
	Linoleic Acid	−6,1
	Myosmine	−6,2
	Niacinamide	−5,5
	Nicotine	−6,1
	Nicotinic Acid	−5,6
	Norcotinine	−6,4
	Nornicotine	−6,3
	Rutin	**−9,8**
1ZKL (PDE7)	Anabasine	−6,4
	Anatabine	−6,4
	Chlorogenic Acid	**−9,4**
	Cotinine	−6,3
	Ferulic Acid	−7,4
	Linoleic Acid	−6,7
	Myosmine	−6,1
	Niacinamide	−5,9
	Nicotine	−6,1
	Nicotinic Acid	−5,6
	Norcotinine	−6,6
	Nornicotine	−6,1
	Rutin	**−11,0**

Macromolecule Target	Bioactive Compound	Binding Energy (kcal/mol)
5HI3 (IL-17A)	Anabasine	−6,2
	Anatabine	−6,1
	Chlorogenic Acid	**−8,0**
	Cotinine	−5,3
	Ferulic Acid	−7,0
	Linoleic Acid	−6,3
	Myosmine	−5,1
	Niacinamide	−5,2
	Nicotine	−5,3
	Nicotinic Acid	−5,2
	Norcotinine	−6,3
	Nornicotine	−6,1
	Rutin	**−9,7**
2AZ5 (TNF-α)	Anabasine	−5,8
	Anatabine	−5,8
	Chlorogenic Acid	**−7,1**
	Cotinine	−6,6
	Ferulic Acid	−5,9
	Linoleic Acid	−5,5
	Myosmine	−5,4
	Niacinamide	−4,9
	Nicotine	−5,7
	Nicotinic Acid	−4,8
	Norcotinine	−6,1
	Nornicotine	−5,8
	Rutin	**−8,4**
6Y8M (IL-1β)	Anabasine	−5,1
	Anatabine	−4,8
	Chlorogenic Acid	**−6,2**
	Cotinine	−5,1
	Ferulic Acid	−5,3
	Linoleic Acid	−4,6
	Myosmine	−4,7
	Niacinamide	−4,4
	Nicotine	−4,6
	Nicotinic Acid	−4,3
	Norcotinine	−4,9
	Nornicotine	−4,8
	Rutin	**−6,9**
4YHK (Prostaglandin E2)	Anabasine	−5,2
	Anatabine	−5,2
	Chlorogenic Acid	**−6,8**
	Cotinine	−4,8
	Ferulic Acid	−6,3
	Linoleic Acid	−5,2
	Myosmine	−5,1
	Niacinamide	−5,0
	Nicotine	−5,3
	Nicotinic Acid	−5,6
	Norcotinine	−4,9
	Nornicotine	−5,2
	Rutin	**−7,8**
1RY8 (Prostaglandin F synthase)	Anabasine	−6,5
	Anatabine	−6,4
	Chlorogenic Acid	**−9,0**
	Cotinine	−6,4
	Ferulic Acid	−6,7
	Linoleic Acid	−6,3
	Myosmine	−5,8
	Niacinamide	−5,4
	Nicotine	−6,2
	Nicotinic Acid	−5,3
	Norcotinine	−6,3
	Nornicotine	−5,8
	Rutin	**−11,0**

Table 3. Detailed molecular docking data concerning bioactive compounds and particular receptors, encompassing COX-1, PDE4, COX-2, PDE7, IL-17A, IL-1β, TNF-α, prostaglandin E2, and prostaglandin F synthase.

Macromolecule Target	Bioactive Compound	Hydrogen Bond	Hydrophobic Interaction	Electrostatic Interaction	2D Visualization
3N8Z (COX-1)	Chlorogenic acid	ARG120:NH2 TYR355:OH MET522:O TYR355:OH SER353:CB LEU352:CD2	GLY526:C,O ALA527:N ALA527	NA	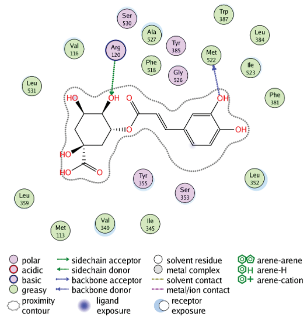
	Rutin	ARG120:NE ARG120:NH2 TYR355:OH SER353:O ALA527:CA SER530:CB	SER353:CA ILE523:CD1 ILE89 LEU115 VAL116 VAL349 LEU352 ILE523 ALA527 VAL349 LEU352 ALA527	NA	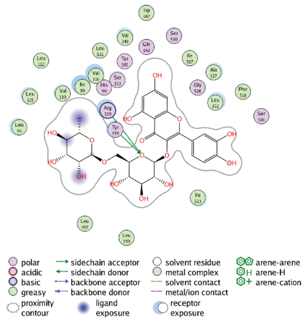
5F1A (COX-2)	Chlorogenic acid	ARG120:NE TYR385:OH MET522:O VAL523:CA SER530:CB TYR355:OH	VAL349 ALA527	NA	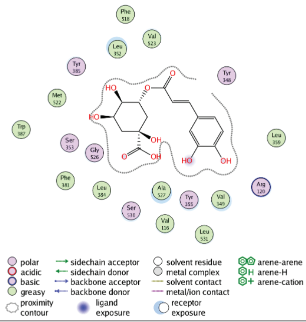
	Rutin	ARG120:NE TYR355:OH TYR385:OH TYR355:OH VAL349:O TYR355:OH TYR385	VAL523:CG1 VAL523:CG2 VAL523:CG2 TYR385 ARG120 LEU352 LEU352 LEU352 MET522 VAL523	NA	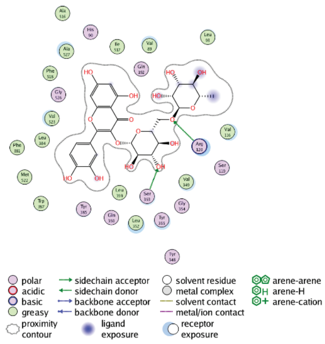
2QYK (PDE4)	Chlorogenic acid	ASP530:OD2 HIS416:NE2 GLU442:OE2 SER420:CA TYR371:OH	TYR371 PHE584 LEU531 ILE548	NA	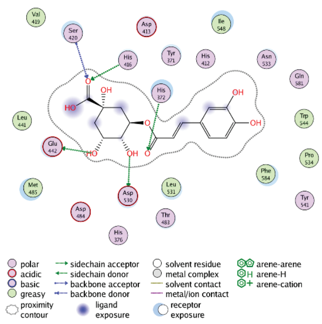

Macromolecule Target	Bioactive Compound	Hydrogen Bond	Hydrophobic Interaction	Electrostatic Interaction	2D Visualization
2QYK (PDE4)	Rutin	ASN533:OD1 THR545:OG1 ASP530:OD2 MET569:SD SER580:O	ILE548:CG2 ILE548:CD1 PHE584 HIS372 MET485	NA	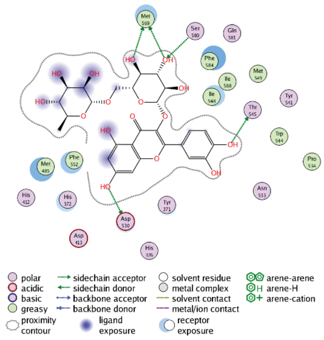
1ZKL (PDE7)	Chlorogenic acid	ASP253:OD1 ASP253:OD1 HIS212:NE2 TYR211:OH HIS212	TYR211 PHE416 VAL380	NA	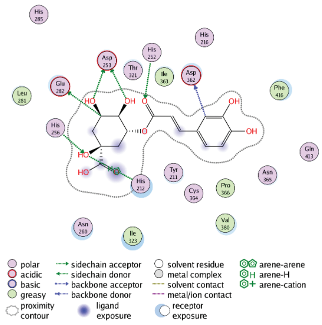
	Rutin	ASN260:ND2 ILE323:N GLN413:NE2 HIS212:NE2 ASP362:OD2 GLN413:OE1 THR321:O ASP253:OD1 ASP253:OD1	PHE416 PHE416 PHE384 PHE384 ILE323 VAL380 ILE323	NA	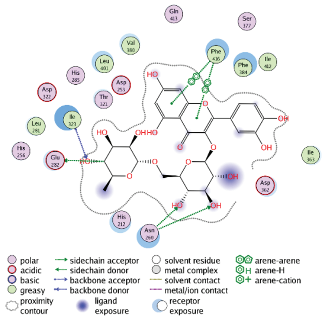
5HI3 (IL-17A)	Chlorogenic acid	ASN36:N TRP67:N LEU97:O LEU97:O VAL65:O VAL65:O PRO63:CD VAL65:O	ILE96:CD1	NA	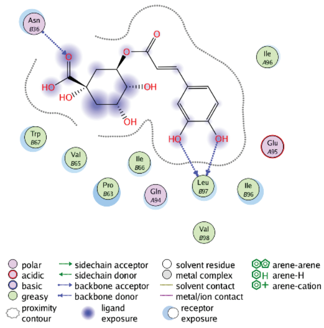
	Rutin	LEU97:N GLU95:O LEU97:O GLU95:OE2 LEU97:O PRO63:CD GLU95:O	ILE96:CA LEU97 LEU97 ILE96	NA	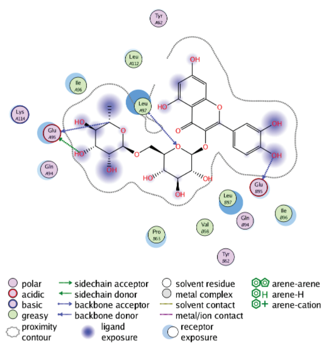

Macromolecule Target	Bioactive Compound	Hydrogen Bond	Hydrophobic Interaction	Electrostatic Interaction	2D Visualization
2AZ5 (TNF-α)	Chlorogenic acid	TYR151:OH GLY121:O TYR119:O TYR119:O TYR119:O LYS98:CE TYR119:O	TYR119	NA	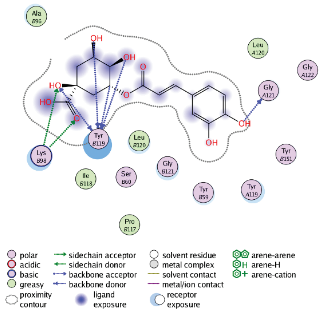
	Rutin	TYR151:OH SER60:O LEU120:O ILE58:O GLY121:CA	TYR119	NA	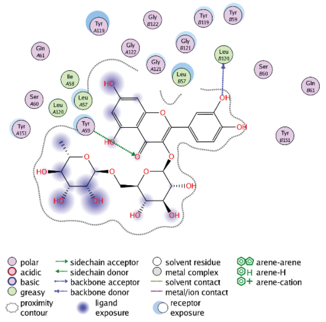
6Y8M (IL-1β)	Chlorogenic acid	ARG11:NE ARG11:NH2 LYS109:NZ GLN149:NE2 MET148:O GLN15:OE1 THR147:OG1 GLN15:OE1 MET148:N	MET148	NA	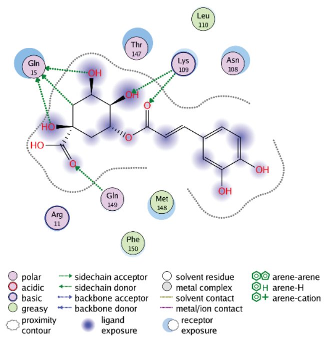
	Rutin	MET148:N MET148:O ASN108:O ASN53:O ASN108:OD1 ASN108:OD1 GLN149:CA	LEU110	LYS103:NZ LYS103:NZ	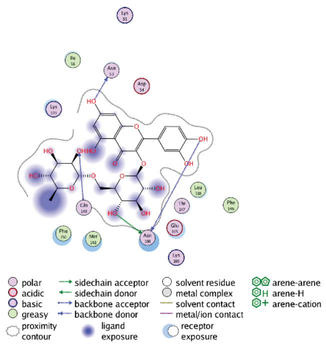
4YHK (Prostaglandin E2)	Chlorogenic acid	TYR33:O TYR103:O ASP104:O	TYR33:CB	NA	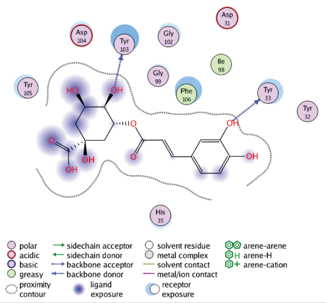

Macromolecule Target	Bioactive Compound	Hydrogen Bond	Hydrophobic Interaction	Electrostatic Interaction	2D Visualization
4YHK (Prostaglandin E2)	Rutin	TYR33:N GLY99:O TYR33:OH GLY99:O	PHE106 TYR33 TYR33 HIS35 TYR33	GLU50:OE1 GLU50:OE2	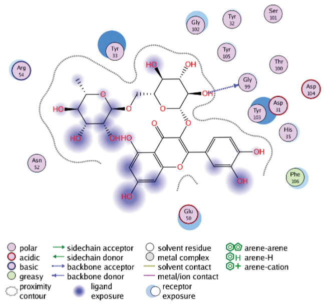
1RY8 (Prostaglandin F synthase)	Chlorogenic acid	SER217:N ALA218:N GLN222:N GLN222:NE2 LYS270:N HIS117:NE2 HIS117:NE2 ALA269:CA TYR55:OH	NA	NA	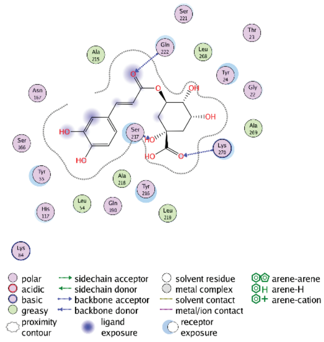
	Rutin	ASN167:ND2 SER221:N LYS270:N ASP50:OD2 ASN167:OD1 TYR216:OH HIS117:NE2 ASP50:OD2 GLN190:OE1 GLN222:NE2	PHE306 TYR24 SER217:C,O ALA218:N LYS270 LYS270	NA	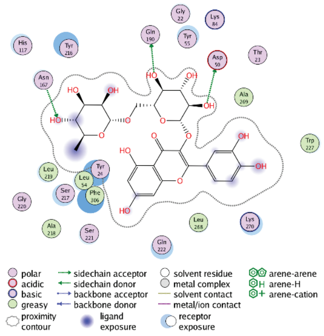

Evaluation of the anti-inflammatory potential of numerous phytochemicals acting via IL-17A underscores the importance of this investigation. These findings underscore the ability of the investigated natural compounds to bind to IL-17A receptors, modulating inflammation response pathways. Further exploration is necessary to ascertain the biological impacts of *Nicotiana tabacum* L. chemical constituents on these cytokines. Interleukin-1 beta and tumor necrosis factor-alpha are critical promoters of inflammation cytokines implicated in a spectrum of inflammatory and immune responses, encompassing conditions including Alzheimer's disease, Crohn's disease, rheumatoid arthritis, and ulcerative colitis. As a result, inhibitors designed to target TNF-α and IL-1β have been created as anti-inflammatory treatments for these disorders (Lee et al. 2002).

Compounds found in *Nicotiana tabacum* L. plants displayed notable interactions against TNF-α, exhibiting a top binding energy of −8.4 kcal/mol. Residues TYR151:OH, SER60:O, LEU120:O, ILE58:O, and GLY121:CA within TNF-α exhibited significant interactions primarily through hydrogen bonds, alongside one hydrophobic interaction involving TYR119 residue. Moreover, the rutin compound demonstrated the ability to establish seven hydrogen bonds with residues MET148:N, MET148:O, ASN108:O, ASN53:O, ASN108:OD1, ASN108:OD1, and GLN149:CA from IL-1β, along with one hydrophobic interaction against LEU110 residue. These results indicate that although tobacco plants successfully suppress TNF-α and IL-1, their impact on their anti-inflammatory effects is relatively modest. TNF-α and IL-1 exhibit weaker interactions with these compounds than they do with their natural ligands, IL-1 receptor and TNF receptor 1 (TNFR1), respectively, suggesting that these bioactive compounds may not disrupt the normal signaling of these cytokines (Souza et al. 2023).

Prostaglandin F synthase (PGFS) belongs to the aldo-keto reductase (AKR) enzyme superfamily, which catalyzes the transformation of prostaglandin D2 (PGD2) into prostaglandin F2α (PGF2α), with Rutin exhibiting a binding energy of −7.8 kcal/mol. Additionally, hydrophobic interactions involve four hydrogen bonds (TYR33:N, GLY99:O, TYR33:OH, and GLY99:O), alongside amino acid residues PHE106, TYR33, TYR33, HIS35, and TYR33, and two electrostatic interactions against GLU50:OE1 and GLU50:OE2 residues. These electrostatic interactions enhance the stability of the PGFS-Rutin complex, thus amplifying Rutin's efficacy in inhibiting PGFS enzyme activity. Throughout this research, the bioactive substances demonstrated a broad spectrum of interaction with COX-1, PDE4, COX-2, PDE7, IL-17A, IL-1β, TNF-α, prostaglandin E2, and prostaglandin F synthase receptors. These macromolecules are crucial in numerous pathological and physiological processes, including cellular signaling, immune responses, inflammation, and pain. Furthermore, Table 3 outlines the docking configurations of the 2D models depicting all bioactive compounds sourced from *Nicotiana tabacum* L. interacting with these receptors.

ADMET and drug-likeness prediction

Table 4 displays the outcomes of ADME forecasts for three substances on the Swiss ADME server. ADME stands for absorption, distribution, metabolism, and excretion. These four key processes dictate how a drug is taken up, dispersed, metabolized, and eliminated by the body (Ahmad et al. 2023). Compounds derived from the tobacco plant (*Nicotiana tabacum* L.) with substantial GI absorption are anticipated to traverse the blood-brain barrier (BBB). They are also anticipated to function as substances that serve as substrates for the P-glycoprotein (Pgp) transporter, which is an efflux transporter able to remove drugs from cells. Moreover, these compounds are anticipated to act as inhibitors of CYP2C9, CYP2C19, and CYP1A2, which are key cytochrome P450 enzymes responsible for metabolic processes. Lastly, these compounds exhibit negative log Kp values, indicating poor skin permeation. Chologenic acid and rutin, possessing low GI absorption, are not projected to penetrate the BBB or act as substrates for Pgp or inhibitors of CYP enzymes. These substances also exhibit negative log Kp values, indicating poor skin permeation. These findings can facilitate the design of drug compounds possessing distinct characteristics. For instance, if a drug that can penetrate the blood-brain barrier (BBB) is required, it is essential to steer clear of compounds forecasted as Pgp substrates or CYP enzyme inhibitors. Similarly, in pursuit of a drug with favorable skin permeability, compounds with high negative log Kp values should be disregarded (Muchtaridi et al. 2018).

Table 5 presents the predictions of drug suitability for all the bioactive compounds. As far as we know, the bioactive compounds found in *Nicotiana tabacum* L. have not been tested in humans yet. Their molecular weights vary from 122.12 g/mol to 610.5 g/mol, exhibiting a different count of rotatable bonds (ranging from 1 to 14), hydrogen bond acceptors (ranging from 2 to 16), and hydrogen bond donors (ranging from 0 to 10). The total polar surface areas span from 16.13 Å^2 to 269.43 Å^2, and the consensus log P values range from −1.29 to 5.45. Among them, only Rutin violates Lipinski's rule (MW>500, NorO>10, NHorOH>5), highlighting possible concerns regarding oral bioavailability and metabolic stability, as evidenced by its low bioavailability score of 0.17. Rutin has a synthetic accessibility score of 6.52, indicating that it is somewhat difficult to synthesize. Chlorogenic acid, a naturally occurring compound recognized for its notable anti-inflammatory and antioxidant effects, has a molecular weight of 354.31 g/mol, featuring five rotatable bonds, nine hydrogen bond acceptors, and six hydrogen bond donors. It violates one Lipinski rule (NHorOH>5) but remains compliant with other criteria. This also suggests potential concerns regarding metabolic stability and oral bioavailability. Its bioavailability score stands at 0.11, while its synthetic accessibility is measured at 4.16, indicating relative difficulty in synthesis.

Overall, the entirety of bioactive compounds displays certain characteristics akin to drugs and may undergo testing for the creation of novel and promising anti-inflammatory molecules. Forecasts regarding the toxicity of substances found in *Nicotiana tabacum* L. are outlined in Table 6.

Table 4. ADME forecasts generated by SwissADME.

Bioactive Compound	Gastrointestinal Absorption	Blood-Brain Barrier Permeant	P-glycoprotein Substrate	Cytochrome 1A2 Inhibitor	Cytochrome 2C19 Inhibitor	Cytochrome 2C9 Inhibitor	Cytochrome 1A22D6 Inhibitor	Cytochrome 1A23A4 Inhibitor	Skin Permeation (Log Kp)
Anabasine	High	+	–	–	–	–	–	–	−6.60 cm/s
Anatabine	High	+	–	–	–	–	–	–	−6.60 cm/s
Chlorogenic Acid	Low	–	–	–	–	–	–	–	−8.76 cm/s
Cotinine	High	+	–	–	–	–	–	–	−7.60 cm/s
Ferulic Acid	High	+	–	–	–	–	–	–	−6.41 cm/s
Linoleic Acid	High	+	–	+	–	+	–	–	−3.05 cm/s
Myosmine	High	+	–	+	–	–	–	–	−6.77 cm/s
Niacinamide	High	–	–	–	–	–	–	–	−7.31 cm/s
Nicotine	High	+	–	–	–	–	–	–	−6.46 cm/s
Nicotinic Acid	High	+	–	–	–	–	–	–	−6.80 cm/s
Norcotinine	High	–	–	–	–	–	–	–	−7.50 cm/s
Nornicotine	High	+	–	–	–	–	–	–	−7.08 cm/s
Rutin	Low	–	+	–	–	–	–	–	−10.26 cm/s

Table 5. Prediction of drug-likeness from the SwissADME server.

Bioactive Compound	Rotatable Bonds	Hbond Acceptors	Hbond Donors	Total Polar Surface Area (TPSA) (Å²)	Consensus Log P	Lipinski Violations	Bioavailability Score	Synthetic Accessibility
Anabasine	1	2	1	24.92	1.52	+	0.55	2.07
Anatabine	1	2	1	24.92	1.35	+	0.55	2.71
Chlorogenic Acid	5	9	6	164.75	−0.38	+	0.11	4.16
Cotinine	1	2	0	33.20	0.82	+	0.55	2.02
Ferulic Acid	3	4	2	66.76	1.36	+	0.85	1.93
Linoleic Acid	14	2	1	37.30	5.45	+	0.85	3.10
Myosmine	1	2	0	25.25	1.52	+	0.55	2.22
Niacinamide	1	2	1	55.98	0.12	+	0.55	1.00
Nicotine	1	2	0	16.13	1.50	+	0.55	2.05
Nicotinic Acid	1	3	1	50.19	0.32	+	0.85	1.00
Norcotinine	1	2	1	41.99	0.65	+	0.55	1.92
Nornicotine	1	2	1	24.92	1.13	+	0.55	1.97
Rutin	6	16	10	269.43	−1.29	−	0.17	6.52

Table 6. Forecasting toxicity. Information sourced from the pkCSM server.

Bioactive Compound	AMES Test Toxicity	Maximum Tolerated Dose (Human)	hERG I Inhibitor	hERG II Inhibitor	Oral Acute Toxicity in Rats (LD50)	Oral Chronic Toxicity in Rats (LOAEL)	Hepatotoxicity	Skin Sensitisation	Minnow Toxicity
Anabasine	−	0.643	−	−	2.479	1.668	+	+	1.916
Anatabine	−	0.633	−	−	2.42	1.604	+	+	1.851
Chlorogenic Acid	−	−0.134	−	−	1.973	2.982	−	−	5.741
Cotinine	−	0.803	−	−	2.44	2.193	+	−	2.309
Ferulic Acid	−	1.082	−	−	2.282	2.065	−	−	1.825
Linoleic Acid	−	−0.827	−	−	1.429	3.187	+	+	−1.31
Myosmine	−	0.765	−	−	2.315	1.656	+	+	2.072
Niacinamide	−	1.15	−	−	2.116	2.616	−	−	2.441
Nicotine	−	0.62	−	−	2.432	1.646	+	+	1.777
Nicotinic Acid	−	0.907	−	−	2.24	2.652	−	−	2.222
Norcotinine	−	0.99	−	−	2.462	2.552	+	−	2.006
Nornicotine	−	0.701	−	−	2.408	1.593	+	+	2.286
Rutin	−	0.452	−	+	2.491	3.673	−	−	7.677

These bioactive substances represent potential compounds not yet trialed in humans. There is no anticipation of mutagenicity among them. Their MTD ranges from −0.827 log(mg/kg/day) to 1.15 log(mg/kg/day), all of which are below the standard toxicity threshold. There is no anticipated inhibition of HERG I or HERG II. Their acute toxicity (LD50) values in oral rats range from 1.429 to 2.491, exceeding the standard threshold for toxicity. Furthermore, their chronic toxicity (LOAEL) values in oral rats range from 1.593 to 3.673, surpassing the standard threshold for toxicity. No hepatotoxicity or skin sensitization is expected from these substances.

In general, chologenic acid and rutin stand out as the least risky among all bioactive compounds. They fall below the established toxicity thresholds across all categories. It is crucial to emphasize that these forecasts remain speculative. The real-world response of a drug within the body might deviate from these projections. Hence, the significance of undertaking experimental investigations to validate these forecasts cannot be overstated. Therefore, while these predictions offer valuable insights, thorough experimental validation is essential to guaranteeing the safety and effectiveness of potential therapies. Ultimately, such comprehensive studies serve as the cornerstone for informed decision-making in the development of pharmaceutical interventions.

Receptor-ligand dynamics with Gromacs 2016.3

Following the successful simulation run, trajectory files generated by GROMACS version 2016.3 were evaluated using XMGRACE version 5.1. Two-dimensional plots were examined to assess root-mean-square-fluctuation (RMSF), root-mean-square-deviation (RMSD), radius of gyration (Rg), and hydrogen bond formation throughout a 500 ns simulation duration. It was noted that COX-2 exhibited a higher value of 0.204 nm compared to complexes displaying stable ligand patterns. Variations in the simulations of COX-2 in different environments, water, and in the presence of chlorogenic acid, rutin, and the reference drug celecoxib, values varied between 0.10 and 0.30 nm (Fig. 1A).

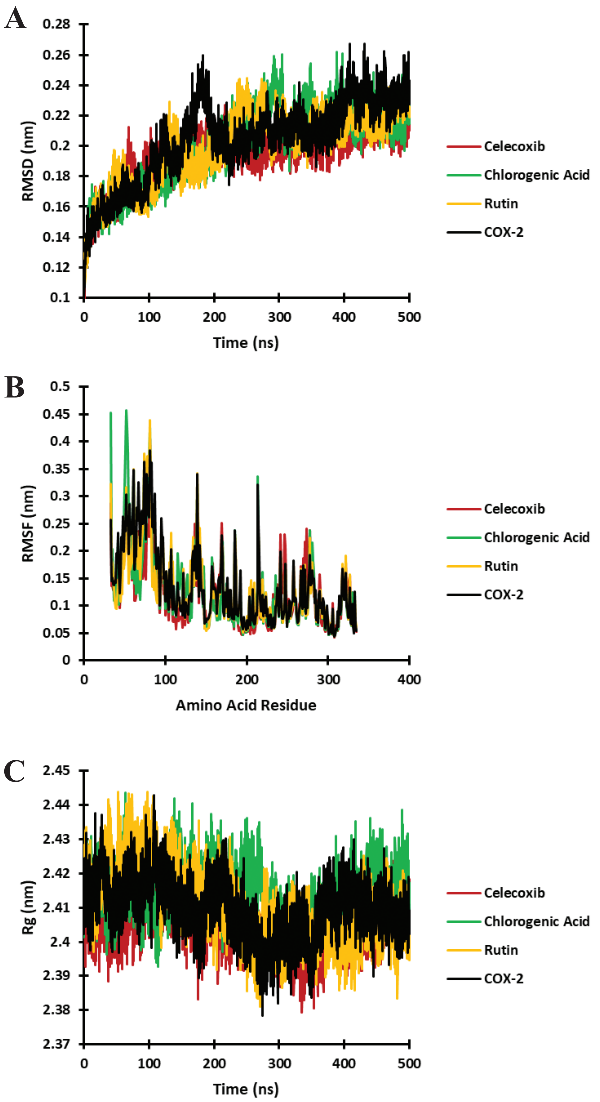

Figure 1. The plots derived from the trajectory file include: **A.** RMSD plot illustrating the deviations for the COX-2-Celecoxib complex (in red), COX-2-Chlorogenic Acid complex (in green), COX-2-Rutin complex (in yellow), and COX-2 in water (in black); **B.** RMSF plot illustrating the fluctuation for each amino acid residue; **C.** The radius of gyration (Rg) plot reflects the level of compactness and tightening of COX-2 in the presence of chlorogenic acid, rutin, and celecoxib.

The COX-2-Celecoxib and COX-2-Rutin complexes exhibited the highest stability, with average measurements of 0.194 nm and 0.199 nm, respectively. RMSF fluctuation values for these complexes varied between 0.05 and 0.50 nm. The average RMSF values recorded for all selected complexes were approximately 0.10 nm, with significant fluctuations noted in certain regions of specific amino acid residues (Fig. 1B). The radius of gyration values indicate the stability and compactness of the proteins' three-dimensional structures, crucial for evaluating protein integrity in the presence of the compounds under investigation. The plots showed radius of gyration values ranging from 2.38 to 2.45 nm for all complexes. Simulations involving COX-2 in water, chlorogenic acid, rutin, and celecoxib displayed nearly identical values approaching 0.11 nm. COX-2 demonstrated slightly higher values around 0.119 nm and remained consistent, with the exception of fluctuations noted during the initial 100 ns of the simulation (Fig. 1C).

Hydrogen bonds are pivotal in ligand-protein interactions and serve as evaluative criteria for studying complex interactions and thermodynamics. Our hydrogen bond analysis revealed that the COX-2-Celecoxib complex established only six hydrogen bonds (6.54%), whereas the COX-2-Chlorogenic Acid complex formed ten bonds (19.74%). Remarkably, the COX-2-Rutin complex demonstrated a significant total of nineteen hydrogen bonds throughout the simulation (106.70%) (Fig. 2). This abundance of hydrogen bonding in the COX-2-Rutin complex suggests strong and potentially stabilizing interactions between Rutin and the COX-2 enzyme active site residues. Such detailed insights into hydrogen bonding patterns contribute to understanding the molecular mechanisms underlying ligand binding and enzyme

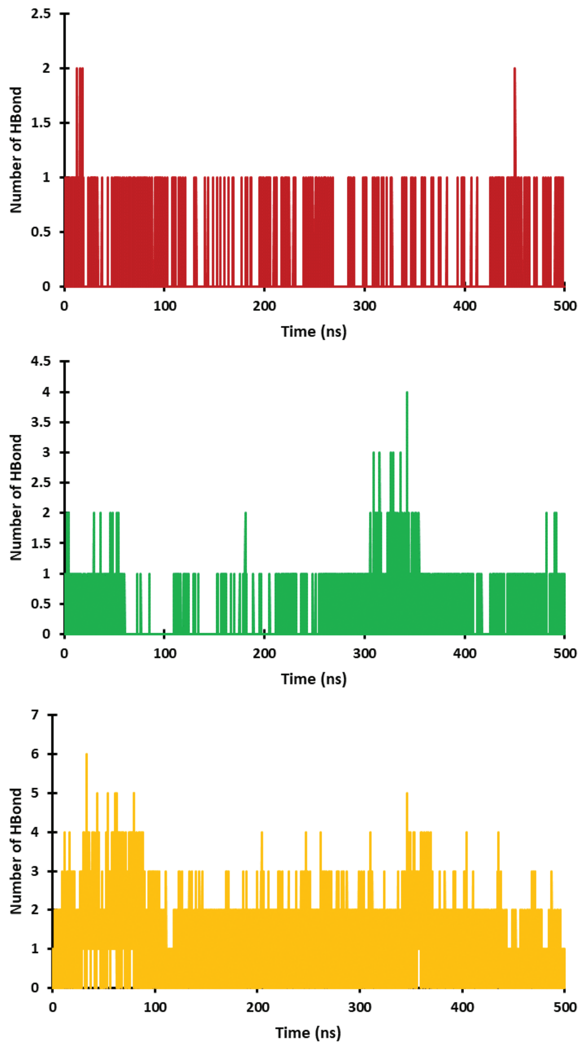

Figure 2. The graph illustrates the count of hydrogen bond interactions observed over a 500 ns simulation period for the chosen complexes: COX-2-Celecoxib complex (depicted in red), COX-2-Chlorogenic Acid complex (shown in green), and COX-2-Rutin complex (represented in yellow).

inhibition, aligning with previous studies emphasizing the significance of hydrogen bonds in ligand-protein interactions (Nurisyah et al. 2024).

Molecular mechanics with poisson–boltzmann surface area (MM-PBSA) method

In this research, the effects of the COX-2-Chlorogenic Acid, COX-2-Rutin, and COX-2-Celecoxib complexes were analyzed concurrently through a comparative evaluation of binding energies, detailed in Table 7. Our results uncover unique binding energy trends (ΔGbind); notably, rutin bound to COX-2 showed a lower binding energy of −141.514 kJ/mol in comparison to chlorogenic acid (−100.609 kJ/mol) and celecoxib (−112.208 kJ/mol). This differential in binding energies suggests varying degrees of affinity and interaction strength between these ligands and the COX-2 enzyme, influencing their potential as inhibitors. Such detailed insights into binding energies are crucial for designing targeted pharmaceutical interventions against inflammatory pathways involving COX-2. Understanding these interactions can pave the way for developing more effective therapeutic strategies aimed at mitigating inflammation-related disorders.

In this study, the interactions and binding affinity of chlorogenic acid and rutin were evaluated, active compounds derived from *Nicotiana tabacum* L. known for their anti-inflammatory effects, involving multiple receptors including COX-1, PDE4, COX-2, PDE7, IL-17A, IL-1β, TNF-α, prostaglandin E2, and prostaglandin F synthase using molecular docking methods. Our findings indicate that chlorogenic acid and rutin selectively inhibit COX-2 more than COX-1, act as dual inhibitors of PDE4 and PDE7, strongly inhibit TNF-α, and moderately inhibit IL-1β. Chlorogenic acid and rutin also demonstrate strong binding affinities with IL-17A, although the biological implications of their interaction with these cytokines remain uncertain. These compounds show promise for treating inflammatory conditions; however, further research is necessary to validate their biological effects.

Table 7. Molecular interaction energies of Celecoxib, Chlorogenic Acid, and Rutin with protein target.

Bioactive Compound	Van der Wall Interaction (kJ/mol)	Electrostatic Interaction (kJ/mol)	Polar Salvation Interaction (kJ/mol)	SASA Interaction (kJ/mol)	Binding Interaction (kJ/mol)
Celecoxib	−219.509 +/− 10.760	−24.000 +/− 9.569	151.248 +/− 9.801	−19.947 +/− 0.722	−112.208 +/− 14.797
Chlorogenic Acid	−205.303 +/− 10.741	−24.536 +/− 17.051	148.107 +/− 15.058	−18.877 +/− 0.691	−100.609 +/− 12.214
Rutin	−316.852 +/− 21.633	−110.981 +/− 19.795	316.533 +/− 18.270	−30.214 +/− 1.021	−141.514 +/− 22.253

Conclusion

Computational methods were utilized to evaluate the binding interactions of bioactive compounds from *Nicotiana tabacum* L. with key inflammatory receptors, including COX-1, PDE4, COX-2, PDE7, IL-17A, IL-1β, TNF-α, prostaglandin E2, and prostaglandin F synthase. The results indicate selective inhibition of COX-2 over COX-1, which is crucial for reducing inflammation while minimizing adverse effects. Additionally, dual inhibition of PDE4 and PDE7 was observed, along with moderate binding affinity with IL-17A, suggesting potential anti-inflammatory benefits. However, the compounds displayed weak binding affinity against TNF-α and IL-1β, implying limited influence on those inflammatory pathways. These findings underscore the potential of the compounds for treating inflammatory conditions, particularly through COX-2 inhibition. Further validation through experimental studies is necessary to confirm these interactions. The promising results warrant additional investigation to optimize these compounds for drug development. This work provides valuable data for anti-inflammatory drug discovery, especially for natural compounds with selective receptor targeting.

Author contributions

Conceptualization, V.M.P., A.F.H., and T.M.F.; methodology, A.F.H., and T.M.F.; software, A.F.H., and T.M.F.; validation, A.F.H., and T.M.F.; formal analysis, A.F.H., and T.M.F.; investigation, A.F.H., and T.M.F.; resources, A.F.H., and T.M.F.; data curation, A.F.H., and T.M.F.; writing – original-draft preparation, V.M.P., A.F.H., and T.M.F.; writing – review and editing, V.M.P., A.F.H., and T.M.F.; visualization, T.M.F.; supervision, V.M.P., A.F.H., and T.M.F. All authors have read and agreed to the published version of the manuscript.

Funding

This research was funded by the Institute for Research and Community Service (LPPM) at Universitas Islam Bandung through the Penelitian Dosen Utama – Penelitian Dasar 2024 grant, under reference No. 220/B.04/LPPM/XII/2023.

Conflicts of interest

The authors declare that there are no conflicts of interest.

Acknowledgments

The authors would like to express their sincere gratitude to the Institute for Research and Community Service (LPPM) at Universitas Islam Bandung for providing financial support for this research through the Penelitian Dosen Utama – Penelitian Dasar 2024 grant, under reference No. 220/B.04/LPPM/XII/2023.

References

Abraham M, Hess B, van der Spoel D, Lindahl E (2015) Gromacs – Reference Manual Version 2016.3. SpringerReference.

Ahmad I, Khan H, Serdaroğlu G (2023) Physicochemical properties, drug likeness, ADMET, DFT studies, and in vitro antioxidant activity of oxindole derivatives. Computational Biology and Chemistry 104: 107861. https://doi.org/10.1016/j.compbiolchem.2023.107861

Ahmad S, Raza S, Uddin R, Azam SS (2018) Comparative subtractive proteomics based ranking for antibiotic targets against the dirtiest superbug: *Acinetobacter baumannii*. Journal of Molecular Graphics and Modelling 82: 74–92. https://doi.org/10.1016/j.jmgm.2018.04.005

Ahrazem O, Zhu C, Huang X, Rubio-Moraga A, Capell T, Christou P, Gómez-Gómez L (2022) Metabolic engineering of crocin biosynthesis in *Nicotiana* Species. Frontiers in Plant Science 13. https://doi.org/10.3389/fpls.2022.861140

Amaro RE, Baudry J, Chodera J, Demir Ö, McCammon JA, Miao Y, Smith JC (2018) Ensemble docking in drug discovery. Biophysical Journal 114(10): 2271–2278. https://doi.org/10.1016/j.bpj.2018.02.038

Aragones JL, Noya EG, Valeriani C, Vega C (2013) Free energy calculations for molecular solids using GROMACS. Journal of Chemical Physics. https://doi.org/10.1063/1.4812362

Bensalah A, Aboufatima R, Benharref A, Chait A (2009) Analgesic and anti-inflammatory activities of *Nicotiana rustica* total extract. Pharmaceutical Biology 47. https://doi.org/10.1080/13880200902896020

BIOVIA (2017) Dassault Systèmes BIOVIA, Discovery Studio Modeling Environment, Release 2017. Dassault Systèmes San Diego.

Bugnon M, Goullieux M, Röhrig UF, Perez MAS, Daina A, Michielin O, Zoete V (2023) SwissParam 2023: A modern web-based tool for efficient small molecule parametrization. Journal of Chemical Information and Modeling 63. https://doi.org/10.1021/acs.jcim.3c01053

Camlica M, Yaldiz G (2021) Analyses and evaluation of the main chemical components in different tobacco (*Nicotiana tabacum* L.) genotypes. Grasas y Aceites 72(1). https://doi.org/10.3989/gya.0801192

Chakraborty AJ, Mitra S, Tallei TE, Tareq AM, Nainu F, Cicia D, Dhama K, Emran T Bin, Simal-Gandara J, Capasso R (2021) Bromelain a potential bioactive compound: A comprehensive overview from a pharmacological perspective. Life 11(4): 317. https://doi.org/10.3390/life11040317

Daina A, Michielin O, Zoete V (2017) SwissADME: A free web tool to evaluate pharmacokinetics, drug-likeness and medicinal chemistry friendliness of small molecules. Scientific Reports 7: 42717. https://doi.org/10.1038/srep42717

Drapal M, Enfissi EMA, Fraser PD (2022) The chemotype core collection of genus *Nicotiana*. Plant Journal 110(5): 1516–1528. https://doi.org/10.1111/tpj.15745

Fioranelli M, Roccia MG, Flavin D, Cota L (2021) Regulation of inflammatory reaction in health and disease. International Journal of Molecular Sciences 22(10): 5277. https://doi.org/10.3390/ijms22105277

Forli W, Halliday S, Belew R, Olson A (2012) AutoDock Version 4.2. Citeseer.

Genheden S, Ryde U (2015) The MM/PBSA and MM/GBSA methods to estimate ligand-binding affinities. Expert Opinion on Drug Discovery 10. https://doi.org/10.1517/17460441.2015.1032936

Gu J, Zhang X, Song B, Zhou D, Niu Y, Cheng G, Zheng Y, Wang Y (2022) Chemical composition of tobacco seed oils and their antioxidant, anti-Inflammatory, and whitening activities. Molecules 27(23): 8516. https://doi.org/10.3390/molecules27238516

He MM, Smith AS, Oslob JD, Flanagan WM, Braisted AC, Whitty A, Cancilla MT, Wang J, Lugovskoy AA, Yoburn JC, Fung AD, Farrington G, Eldredge JK, Day ES, Cruz LA, Cachero TG, Miller SK, Friedman JE, Choong IC, Cunningham BC (2005) Medicine: Small-molecule inhibition of TNF-α. Science 310. https://doi.org/10.1126/science.1116304

Huang JX, Zhu BL, Xu JP, Zhou ZZ (2023) Advances in the development of phosphodiesterase 7 inhibitors. European Journal of Medicinal Chemistry 250: 115–194. https://doi.org/10.1016/j.ejmech.2023.115194

Jin Z, Wu X, Liu H, Xu C (2020) Celecoxib, a selective COX-2 inhibitor, markedly reduced the severity of tamoxifen-induced adenomyosis in a murine model. Experimental and Therapeutic Medicine 19(5): 3289–3299. https://doi.org/10.3892/etm.2020.8580

Komoto J, Yamada T, Watanabe K, Takusagawa F (2004) Crystal Structure of Human Prostaglandin F Synthase (AKR1C3). Biochemistry 43. https://doi.org/10.1021/bi036046x

Kumari R, Kumar R, Consortium OSDD, Lynn A (2014) g _ mmpbsa – A GROMACS tool for MM-PBSA and its optimization for high-throughput binding energy calculations. Journal of Chemical Information and Modeling. https://doi.org/10.1021/ci500020m

Laszlo C, Kaminski K, Guan H, Fatarova M, Wei J, Bergounioux A, Schlage WK, Schorderet-Weber S, Guy PA, Ivanov NV, Lamottke K, Hoeng J (2022) Fractionation and extraction optimization of potentially valuable compounds and their profiling in six varieties of two *Nicotiana* species. Molecules 27(22): 8105. https://doi.org/10.3390/molecules27228105

Leal M, Moreno MA, Albornoz PL, Mercado MI, Zampini IC, Isla MI (2023) *Nicotiana tabacum* leaf waste: morphological characterization and chemical-functional analysis of extracts obtained from powder leaves by using green solvents. Molecules 28(3): 1396. https://doi.org/10.3390/molecules28031396

Lee YB, Nagai A, Kim SU (2002) Cytokines, chemokines, and cytokine receptors in human microglia. Journal of Neuroscience Research 69(1): 94–103. https://doi.org/10.1002/jnr.10253

Liu S, Dakin LA, Xing L, Withka JM, Sahasrabudhe P V., Li W, Banker ME, Balbo P, Shanker S, Chrunyk BA, Guo Z, Chen JM, Young JA, Bai G, Starr JT, Wright SW, Bussenius J, Tan S, Gopalsamy A, Lefker BA, Vincent F, Jones LH, Xu H, Hoth LR, Geoghegan KF, Qiu X, Bunnage ME, Thorarensen A (2016) Binding site elucidation and structure guided design of macrocyclic IL-17A antagonists. Scientific Reports 6: 30859. https://doi.org/10.1038/srep30859

Lucido MJ, Orlando BJ, Vecchio AJ, Malkowski MG (2016) Crystal structure of aspirin-acetylated human cyclooxygenase-2: insight into the formation of products with reversed stereochemistry. Biochemistry 55. https://doi.org/10.1021/acs.biochem.5b01378

Mohapatra S, Prasad A, Haque F, Ray S, De B, Ray SS (2015) *In silico* investigation of black tea components on α-amylase, α-glucosidase and lipase. Journal of Applied Pharmaceutical Science 5(12): 42–47. https://doi.org/10.7324/JAPS.2015.501207

Moore SC, Vaz de Castro PAS, Yaqub D, Jose PA, Armando I (2023) Anti-inflammatory effects of peripheral dopamine. International Journal of Molecular Sciences 24(18): 13816. https://doi.org/10.3390/ijms241813816

Muchtaridi M, Dermawan D, Yusuf M (2018) Molecular docking, 3D structure-based pharmacophore modeling, and ADME prediction of alpha mangostin and its derivatives against estrogen receptor alpha. Journal of Young Pharmacists 10(3): 252–259. https://doi.org/10.5530/jyp.2018.10.58

Nacoulma AP, Compaoré M, de Lorenzi M, Kiendrebeogo M, Nacoulma OG (2012) In vitro antioxidant and anti-inflammatory activities of extracts from *Nicotiana tabacum* L. (Solanaceae) leafy galls induced by rhodococcus fascians. Journal of Phytopathology 160. https://doi.org/10.1111/j.1439-0434.2012.01953.x

Nurisyah, Ramadhan DSF, Dewi R, Asikin A, Daswi DR, Adam A, Chaerunnimah, Sunarto, Rafika, Artati, Fakih TM (2024) Targeting EGFR allosteric site with marine-natural products of Clathria Sp.: A computational approach. Current Research in Structural Biology 7: 100–125. https://doi.org/10.1016/j.crstbi.2024.100125

Park M, Kim D, Ko S, Kim A, Mo K, Yoon H (2022) Breast cancer metastasis: mechanisms and therapeutic implications. International Journal of Molecular Sciences 23(12): 6806. https://doi.org/10.3390/ijms23126806

Pires DEV, Blundell TL, Ascher DB (2015) pkCSM: Predicting small-molecule pharmacokinetic and toxicity properties using graph-based signatures. Journal of Medicinal Chemistry 58. https://doi.org/10.1021/acs.jmedchem.5b00104

Popova VT, Ivanova TA, Stoyanova AS, Nikolova VV, Docheva MH, Hristeva TH, Damyanova ST, Nlkolov NP (2020) Chemical constituents in leaves and aroma products of nicotiana rustica L. Tobacco. International Journal of Food Studies 9(1). https://doi.org/10.7455/IJFS/9.1.2020.A2

Radovanović K, Gavarić N, Aćimović M (2023) Anti-inflammatory properties of plants from serbian traditional medicine. Life 13(4): 874. https://doi.org/10.3390/life13040874

Rivera-García LG, Francis-Malavé AM, Castillo ZW, Uong CD, Wilson TD, Ferchmin PA, Eterovic V, Burton MD, Carrasquillo Y (2024) Anti-hyperalgesic and anti-inflammatory effects of 4R-tobacco cembranoid in a mouse model of inflammatory pain. Journal of Inflammation (United Kingdom) 21(2). https://doi.org/10.1186/s12950-023-00373-8

Sapay N, Tieleman DP (2011) Combination of the CHARMM27 force field with united-atom lipid force fields. Journal of Computational Chemistry 32(7): 1400–1410. https://doi.org/10.1002/jcc.21726

Schiele F, van Ryn J, Litzenburger T, Ritter M, Seeliger D, Nar H (2015) Structure-guided residence time optimization of a dabigatran reversal agent. mAbs 7. https://doi.org/10.1080/19420862.2015.1057364

Secchi F, Schubert A, Lovisolo C (2016) Changes in air CO2 concentration differentially alter transcript levels of NTAQP1 and NTPIP2;1 aquaporin genes in tobacco leaves. International Journal of Molecular Sciences 17(4): 567. https://doi.org/10.3390/ijms17040567

Sidhu RS, Lee JY, Yuan C, Smith WL (2010) Comparison of cyclooxygenase-1 crystal structures: Cross-talk between monomers comprising cyclooxygenase-1 homodimers. Biochemistry 49. https://doi.org/10.1021/bi1003298

Souza RF, Caetano MAF, Magalhães HIR, Castelucci P (2023) Study of tumor necrosis factor receptor in the inflammatory bowel disease. World Journal of Gastroenterology 29(18): 2733–2746. https://doi.org/10.3748/wjg.v29.i18.2733

von Stebut E, Boehncke WH, Ghoreschi K, Gori T, Kaya Z, Thaci D, Schäffler A (2020) IL-17A in psoriasis and beyond: cardiovascular and metabolic implications. Frontiers in Immunology 10: 3096. https://doi.org/10.3389/fimmu.2019.03096

Turner P (2005) XMGRACE, Version 5.1. 19. Center for coastal and land-margin research, Oregon Graduate Institute of Science and Technology, Beaverton.

Vanommeslaeghe K, Hatcher E, Acharya C, Kundu S, Zhong S, Shim J, Darian E, Guvench O, Lopes P, Vorobyov I, Mackerell AD (2010) CHARMM general force field: A force field for drug-like molecules compatible with the CHARMM all-atom additive biological force fields. Journal of Computational Chemistry 31(4): 671–690. https://doi.org/10.1002/jcc.21367

Wang H, Liu Y, Chen Y, Robinson H, Ke H (2005) Multiple elements jointly determine inhibitor selectivity of cyclic nucleotide phosphodiesterases 4 and 7. Journal of Biological Chemistry 280(35): 30949–30955. https://doi.org/10.1074/jbc.M504398200

Wang H, Peng MS, Chen Y, Geng J, Robinson H, Houslay MD, Cai J, Ke H (2007) Structures of the four subfamilies of phosphodiesterases provide insight into the selectivity of their inhibitors. Biochemical Journal 408(2): 193–201. https://doi.org/10.1042/BJ20070970

Yasmin R, Siraj S, Hassan A, Khan AR, Abbasi R, Ahmad N (2015) Epigenetic regulation of inflammatory cytokines and associated genes in human malignancies. Mediators of Inflammation 2015: 201703. https://doi.org/10.1155/2015/201703

Zhang W, Lin H, Zou M, Yuan Q, Huang Z, Pan X, Zhang W (2022a) Nicotine in inflammatory diseases: anti-inflammatory and pro-inflammatory effects. Frontiers in Immunology 13: 826889. https://doi.org/10.3389/fimmu.2022.826889

Zhang X, Zhang L, Zhang J, Jia M, Cao L, Yu J, Zhao D (2022b) Haploid induction in allotetraploid tobacco using DMPs mutation. Planta 255: 98. https://doi.org/10.1007/s00425-022-03877-4